

Gain Enhancement of a Dual-Band Planar Slot Dipole using AMC Plane for WBAN and WLAN Applications

Fatin Nabilah Gimán¹, Ping Jack Soh^{1,5}, Mohd Faizal Jamlos², Herwansyah Lago³, Azremi Abdullah Al-Hadi¹, Sharul Kamal Abdul Rahim⁴, Dominique Schreurs⁵, Prayoot Akkaraekthalin⁶, and Adalbert Beyer⁷

¹ Advanced Communication Engineering Centre (ACE), School of Computer and Communication Engineering Universiti Malaysia Perlis (UniMAP), Pauh Putra, 02600, Arau, Perlis, Malaysia
pjs@unimap.edu.my

² Faculty of Mechanical Engineering, Universiti Malaysia Pahang, 26600 Pekan, Pahang, Malaysia

³ Faculty of Engineering, Universiti Malaysia Sabah, 88400 Kota Kinabalu, Sabah, Malaysia

⁴ Wireless Communication Center (WCC), Universiti Teknologi Malaysia, 81310 UTM Skudai, Johor, Malaysia

⁵ ESAT-TELEMIC Research Division, KU Leuven, Kasteelpark Arenberg 10 Box 2444, 3001 Leuven, Belgium

⁶ Department of Electrical and Computer Engineering, Faculty of Engineering King Mongkut's University of Technology North Bangkok, (KMUTNB) 1518 Pracharat 1 Rd., Wongsawang, Bangsue, Bangkok, 10800 Thailand

⁷ High Frequency Engineering (HFT), University Duisburg-Essen, Bismarckstrasse 81, 47057 Duisburg, Germany

Abstract — A dual band slot dipole antenna made from textile is proposed for Wireless Body Area Network and Wireless Local Area Network applications. The proposed antenna is integrated with an artificial magnetic conductor plane to mitigate backward radiation and reduce Specific Absorption Rate when operated on body. The artificial magnetic conductor plane is formed using a 3 x 3 array of unit cells, each consisting of a square patch integrated with diamond-shaped slot. The proposed antenna (denoted as Antenna B) is compared against another similar antenna (Antenna A) in free space and on-body, in flat condition (on chest) and under two bending axes (x - and y -axes) on the upper arm. Results indicate that Antenna B provided wider upper bandwidth to 766 MHz (in flat condition) and up to 875 MHz when bent. Besides that, higher gain of up to 5 dB with improved front-to-back ratio are also observed.

Index Terms — Antennas, artificial magnetic conductor, metamaterial, multiband antennas, wearable antennas.

I. INTRODUCTION

Wireless body area network (WBAN) and Wireless Local Area Network are two of the most widely researched applications globally. Their frequencies

include the Industrial Scientific Medical (ISM) band (from 2.4 to 2.48 GHz), Ultra-Wide band (UWB) (from 3.1 to 10.76 GHz), Wireless Local Area Network (WLAN) (in the 2.4 and 5 GHz bands) [1]-[14]. In line with this development, wearable antenna made from flexible materials are also widely investigated due to its attractive features: low profile, flexible, inexpensive, lightweight, and most importantly, safe to be worn. However, when placed on body, an antenna with high back radiation or omnidirectional pattern such as dipole antenna [2] tends to increase the electromagnetic absorption in the human body due to its proximity during operation. This almost certainly results in high SAR value which potentially affect human body tissues. The American National Standards Institute (ANSI) and International Commission on Non-Ionizing radiation Protection (ICNIRP) regulated that the exposure for human tissues is limited to 1.6 W/kg averaged per 1g of tissue and 2 W/kg per 10 g of tissue, respectively.

One of the solutions to control the level of the back-radiation is either by selecting an antenna topology with a rear ground plane or to introduce a metallic plane to function as a reflector. However, conventional reflecting structure interferes antenna operation, and they are typically placed at an extended distance from the

radiator. Such setup, in turn, increases the height of the antenna structure and reduces its suitability to be worn on body due to increased thickness. Moreover, the gap of such structure is frequency-dependent, which requires the gap to be determined based on the lower frequency in the case of a multi-resonance antenna, which again increases the thickness. To overcome this, metasurfaces with dual-band behavior such as Electromagnetic Bandgap (EBG) or Artificial Magnetic Conductor (AMC) can be an ideal solution to balance between thickness and modifying radiation characteristics [3]-[10].

In this paper, a dual-band antenna and a dual-band AMC plane is proposed. The AMC plane is formed using an array of unit cell elements based on a square patch integrated with diamond-shaped slot to enable dual band operation. The optimized antenna (Antenna B) is compared with a previous work [1] (denoted as Antenna A) to assess its improvements in terms of bandwidth, gain and front-to-back ratio. The next section describes the antenna design and materials used, followed by the assessment of their performance in free space and on body. A comprehensive SAR investigation to validate the contribution of the AMC plane is presented prior to the concluding remarks.

II. TEXTILE MATERIALS AND ANTENNA SPECIFICATION

A. Antenna design

Two topologies of the proposed C-slotted dual band textile antenna are shown in Figs. 1 (a) and 1 (b). They operate in the 2.45 GHz (lower) and 5.8 GHz (upper) bands. The proposed antenna is integrated with an AMC layer between its substrate and ground. The previous antenna from [1] (denoted as Antenna A) shown in Fig. 1 (a) is compared with the proposed C-slotted dipole antenna with optimized AMC (denoted as Antenna B) and shown in Fig. 1 (b).

All antennas are designed using the same textile materials. Felt with a thickness of 3 mm is used as its substrate, while ShieldIt Super conductive textile with a thickness of 0.17 mm is used to form the patch, ground and AMC of the proposed antenna. The relative permittivity and loss tangent of the felt substrate is 1.44 and 0.044, respectively, whereas the conductivity of the ShieldIt Super is 1.18×10^5 S/m. To provide a fair comparison, the overall area of both antennas are limited to 90×90 mm² with the same thickness of 6.51 mm. Both antennas are built using five layers of textiles (see Fig. 1 (e)), as follows: a ground layer on the bottom-most layer, followed by two layers of substrate and a layer consisting of the AMC plane in between them. Finally, a patch layer is placed on the top. Their optimized

dimensions are summarized in Table 1.

Table 1: Optimized parameters of the proposed antenna

Antenna/ Parameter Values (mm)	Antenna A (with AMC) [1]	Antenna/ Parameter Values (mm)	Antenna B (Optimized AMC)
L/W	90	La/Wa	90
Ll	45	Lb	47
Wl	55	Wb	62
A	10	a	9
B	30	b	34
C	22	c	26
D	4	d	4
E	16	e	21
F	2	f	2
-	-	g	12
-	-	h	2

In this work, the Finite Integration Technique (FIT) was used, which is a way of generalizing the FDTD method with weak link to the FEM method. The discretization of Maxwell's equations is done on a pair of dual discretization meshes. The degrees of freedom are corresponding to integral types: electrical voltages and magnetic fluxes on the first type of meshes, and magnetic voltages and electrical fluxes on the second type of meshes. The FIT technique can be used in a very wide frequency range from DC to THz, and for many types of meshes, and curved contours. This technique can be used advantageously and very efficiently for the calculation of multilayered structures, as the results of this work show. The numerical work was performed using CST Microwave Studio Suite, which incorporates this method.

B. AMC plane design

The 3×3 array of square patch unit cells integrated with diamond-shaped slots forms the AMC plane. This plane is implemented to reduce back radiation as shown in Figs. 1 (f) and 1 (g). The AMC is designed similar to [1] for a fair comparison and is further optimized to enable zero reflection phase at 2.45 and 5.8 GHz for Antenna B, as shown in Fig. 2. For the optimized AMC, a shorter current path is provided for the AMC to operate in the upper band (5.8 GHz). This resulted in a wider reflection phase bandwidth of 15.8% or 891 MHz (from 5.189 to 6.08 GHz), while the larger current path enables operation at the lower 2.45 GHz frequency. The phase reflection indicated operation with a bandwidth of 7.76% or 187 MHz (from 2.32 to 2.5 GHz). This indicated that the optimized AMC plane for Antenna B improved in terms of wider reflection phase bandwidth in the upper band.

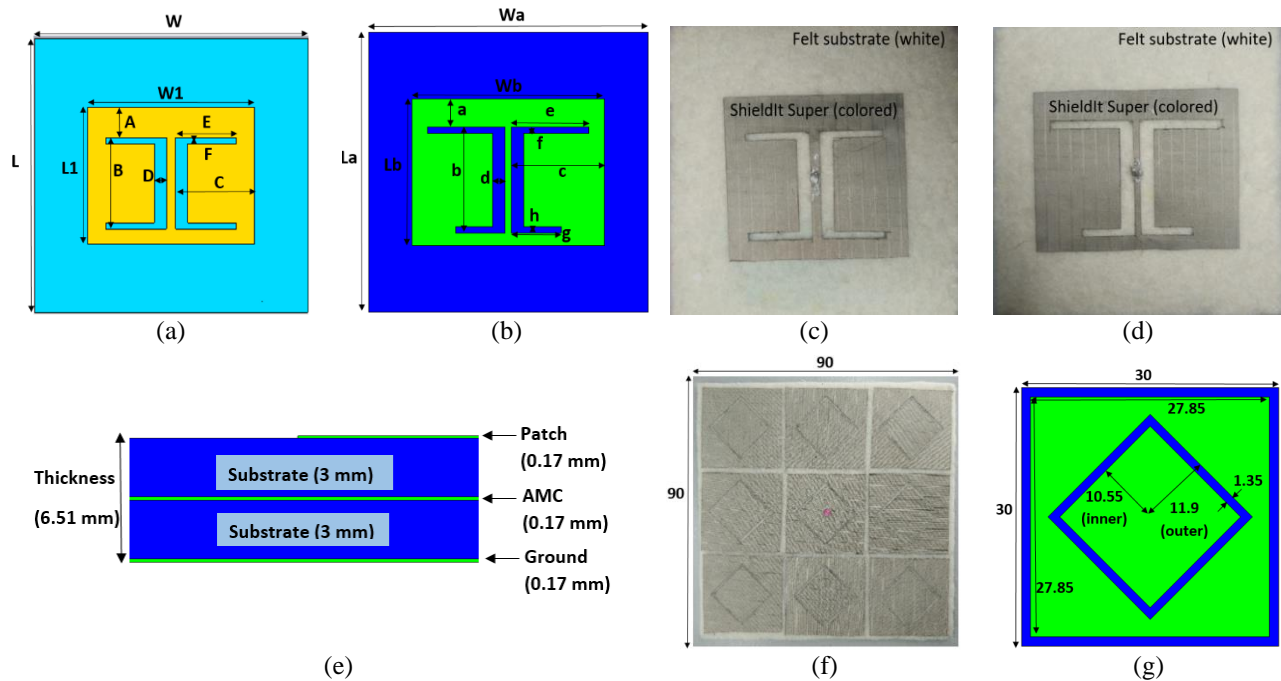


Fig. 1. Topology of the proposed antenna: (a) Antenna A (with AMC) [1], (b) Antenna B (with optimized AMC), (c) fabricated Antenna A, (d) fabricated Antenna B, (e) layer structure of the antenna, (f) fabricated AMC plane from [1], and (g) optimized AMC unit cell dimensions (in mm).

III. RESULTS AND DISCUSSIONS

A. Planar antenna in free space

The performance of both antennas (A and B) in free space are compared and summarized in Table 2. It shows that the simulated reflection coefficient (S_{11}) in free space planar condition for both antennas is below -15 dB and -21 dB in the lower (2.45 GHz) and upper (5.8 GHz) band. The radiation pattern of both antennas in free space and planar condition is directional in the azimuth plane with a maximum directivity of 5.26 dBi (Antenna A) and 7.31 dBi (Antenna B) in the lower band, see Fig. 3. On the other hand, a maximum directivity of 10.7 dBi (for Antenna A) and 9.88 dBi (for Antenna B) is observed in the upper band. Table 2 shows that the realized gain in free space of flat for Antenna A produce a negative realized gain while Antenna B produce a positive realized gain. This indicates that the dissimilar slot length in the radiator and the integration of the optimized AMC plane contributed in improving the gain of Antenna B in the lower band from -2.47 dB to 2.38 dB, a significant increase of about 5 dB. Meanwhile, the realized gain in the upper band for Antenna B is higher than 6 dB. This is slightly lower than the realized gain for Antenna A in

this band (which is about 7 dB) due to the marginal S_{11} at 5.8 GHz for Antenna B. Nonetheless, the simulated front-to-back ratio (FBR) of Antenna B in the flat condition is higher in both bands compared to Antenna A.

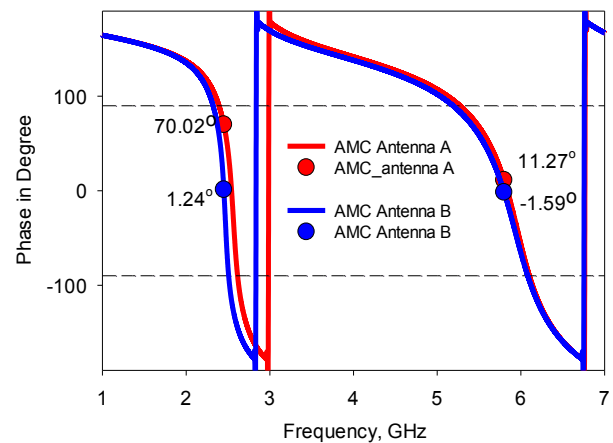


Fig. 2. Simulated reflection phase of the AMC plane for Antenna A [1] and B (proposed). The dotted lines represents the $\pm 90^\circ$ operating range of the AMC plane.

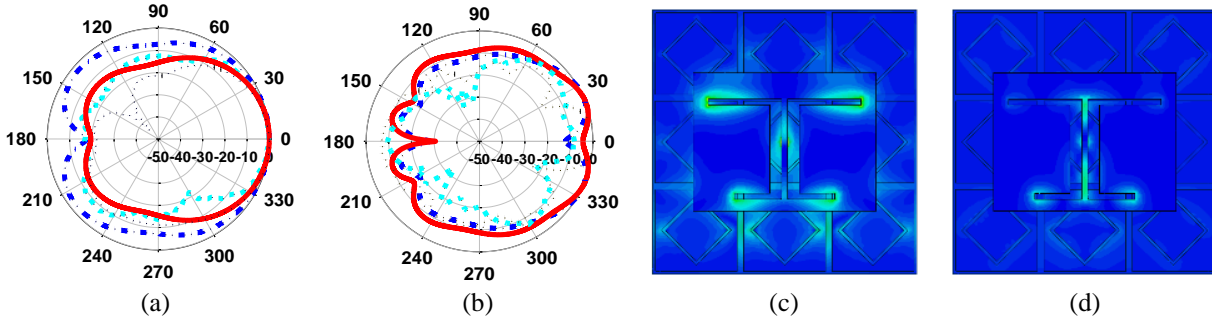


Fig. 3. Simulated and measured radiation pattern in planar free space condition at: (a) 2.45 GHz and (b) 5.8 GHz. Simulated surface currents distribution of Antenna B at: (c) 2.45 GHz and (d) 5.8 GHz. Legend: Dash dot (blue) line: simulated Antenna A, solid (red) line: simulated Antenna B, short dashed (cyan) line: measured Antenna A, dotted (black): measured Antenna B.

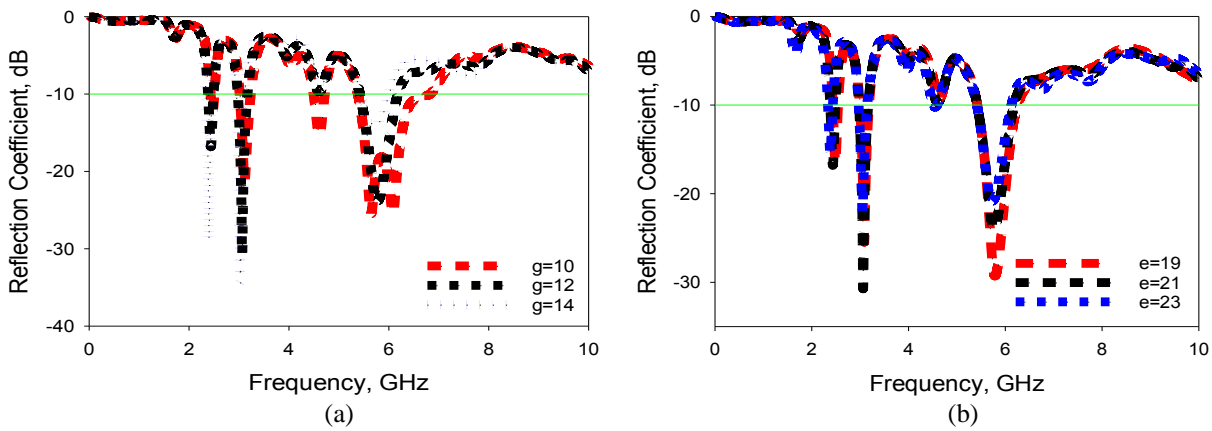


Fig. 4. Effects of the slot lengths on the antenna reflection coefficients: (a) g and (b) e .

The two arms of the slot dipoles are expected to provide tuning for the resonant frequency and impedance matching for the antenna structure, and are investigated. The slot lengths of the two arms are denoted as g and e , and their effects on the antenna performance are investigated. It can be summarized that the length of g highly determines the antenna's resonant frequency, whereas the length of e influences the impedance matching. More specifically, the resonant frequency can be shifted to the lower frequencies by increasing the length of g , as shown in Fig. 4 (a). Meanwhile, an improved impedance matching at the specific resonant frequency can be exhibited by decreasing the length of e , as shown in Fig. 4 (b). For that reason, the lengths of g and e are crucial parameters and must be accurately fabricated.

B. Assessment of antenna in free space under bending

As wearable antennas are designed to be worn on-body, there is always risks of them being operated when bent. To maintain operation in such situations, the

proposed antennas are investigated further when bent in the x - and y -axes with a radius, r of 60 mm in free space, denoted as $X60$ and $Y60$, respectively. Simulated and measured S_{11} of the antenna when bent at both axes are shown in Fig. 5. The maximum realized gains of Antenna B when bent at both axes are improved to 2.25 dB ($X60$) and 1.34 dB ($Y60$) in the lower band. In the upper band, its gains of 5.93 dB is observed under condition $X60$ and 4.48 dB under condition $Y60$. On the contrary, Antenna A exhibited negative realized gains for all bending configurations. Besides that, Antenna B also improved in terms of FBR for both bending configurations. Its FBR are at least 9 dB in the lower band and 22 dB in the upper band. The measured radiation patterns of both antennas when bent in configurations $X60$ and $Y60$ are compared with planar free space in Fig. 6. Both bent antennas at both axes are directional in the azimuth plane with maximum directivities of at least 7 dBi and 9 dBi in the lower and upper bands, respectively.

Table 2: Performance summary of Antennas A and B in the planar and bent configurations

Antenna/Freq./Parameter	Condition	A (with AMC)		B (with optimized AMC)	
	Freq. (GHz)	2.45	5.8	2.45	5.8
S_{11} (dB)	Flat (sim)	-23.91	-22.55	-15.69	-24.55
	Flat (meas)	-5.75	-13.63	-16.41	-8.24
	Chest (meas)	-8.24	-25.51	-13.51	-8.30
	X60 (sim)	-25.18	-23.88	-10.69	-29.26
	X60 (meas)	-9.85	-21.68	-9.96	-7.12
	Y60 (sim)	-21.89	-27.22	-10.68	-34.68
	Y60 (meas)	-7.56	-21.68	-14.44	-8.09
Bandwidth (MHz)	Flat (sim)	123	714	109	766
	Flat (meas)	80	600	50	600
	Chest (meas)	100	870	105	475
	X60 (sim)	121	765	100	875
	X60 (meas)	50	900	55	550
	Y60 (sim)	124	800	104	850
	Y60 (meas)	75	750	80	570
Real. Gain (dB)	Flat (sim)	-2.47	7.17	2.38	6.53
	Flat (meas)	-2.2	9.32	5.89	7.21
	Chest (meas)	-2.87	5.54	3.21	6.99
	X60 (sim)	-1.33	5.96	2.25	5.93
	X60 (meas)	-8.78	5.1	3.96	5.2
	Y60 (sim)	-1.04	5.12	1.34	4.48
	Y60 (meas)	-2.66	-0.29	2.42	-2.54
Front to Back Ratio, FBR (dB)	Flat (sim)	2.74	22.62	17.35	18.8
	Flat (meas)	4.95	28.47	17.14	28.62
	Chest (meas)	6.42	5.54	22.83	22.07
	X60 (sim)	3.59	20.58	8.914	22.87
	X60 (meas)	16.0	16.46	20.89	21.33
	Y60 (sim)	3.76	16.53	10.415	16.71
	Y60 (meas)	7.19	14.50	23.76	4.69
Directivity, (dBi)	Flat (sim)	5.26	10.7	7.31	9.88
	X60 (sim)	5.7	8.41	7.81	8.98
	Y60 (sim)	6.25	9.21	6.5	7.57

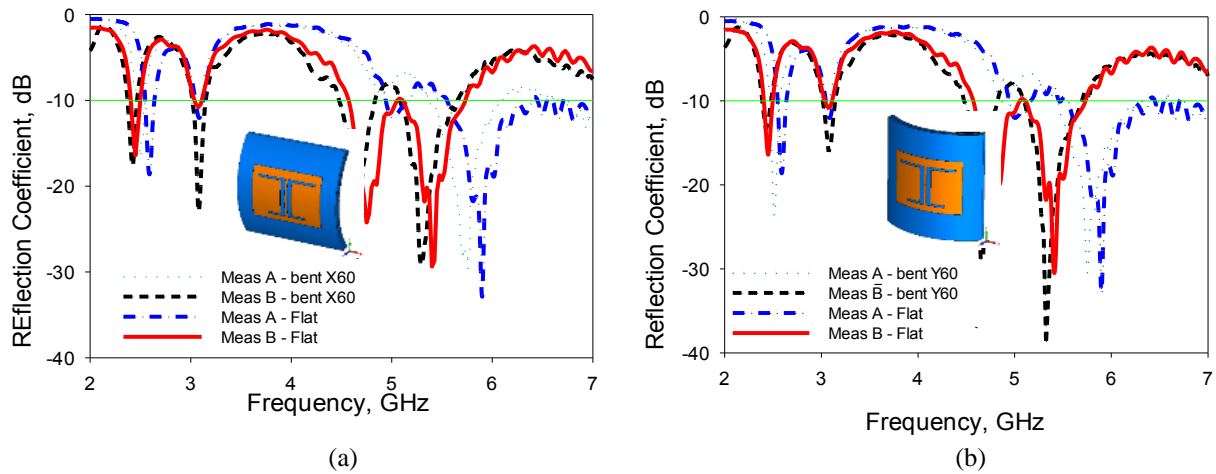


Fig. 5. Measured reflection coefficients of Antenna A and B in free space in planar condition (flat) and (a) under bending with X60; (b) under bending with Y60.

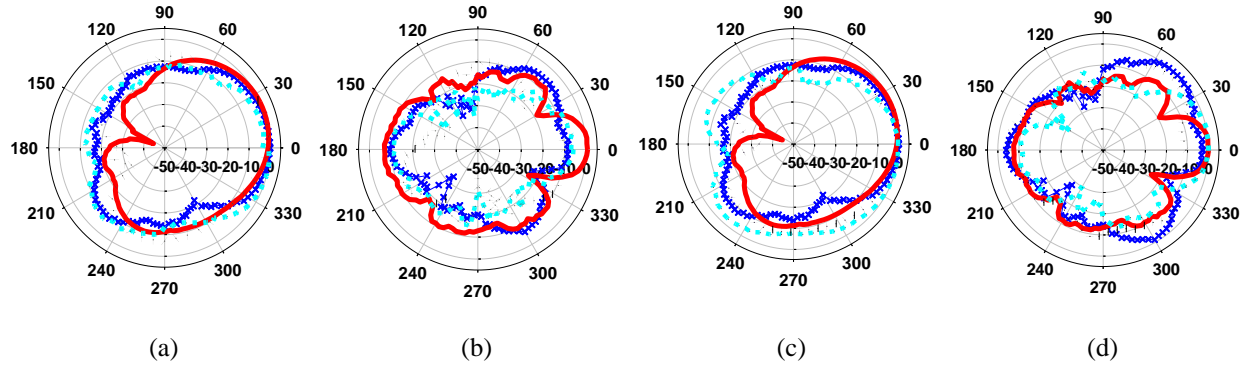


Fig. 6. Normalized measured radiation patterns of Antennas A and B in planar (flat) and when bent with $X60$ and $Y60$ conditions in free space in the xz -plane at (a) 2.45 GHz ($X60$), (b) at 5.8 GHz ($X60$), (c) 2.45 GHz ($Y60$), and (d) 5.8 GHz ($Y60$). Legend: Crossed (blue) line: Antenna A flat, solid (red) line: Antenna B flat, short dash (cyan) line: Antenna A with $X60/Y60$, and dotted (black) line: Antenna B with $X60/Y60$.

C. Assessment of antenna placed on body in flat and under bending conditions

On body assessments were performed on a truncated detailed human body model (in simulations) with in three configurations: (1) in flat condition (on chest); (2) in $X60$ condition on a truncated upper arm; and (3) in $Y60$ condition on the same truncated upper arm. Simulations of the proposed structure on the dispersive tissues were performed using the finite time integral method using voxel resolutions of $2 \times 2 \times 2 \text{ mm}^3$. The chest and the upper arms contain mainly the skin, muscle and fat tissues, which properties are

summarized in Table 3 [15]. Similarly, measurements were performed on a human volunteer on both locations and the three configurations when placed at 10 mm away from the body phantom. To evaluate the level of degradation contributed by the human body, the S_{11} for both antennas are first measured on-body in a flat condition on the chest as shown in Fig. 7. This is compared with its performance when simulated in planar form. Next, the antenna is further evaluated in terms of radiation patterns in an anechoic chamber, and measurements gathered are compared with simulations in Fig. 8.

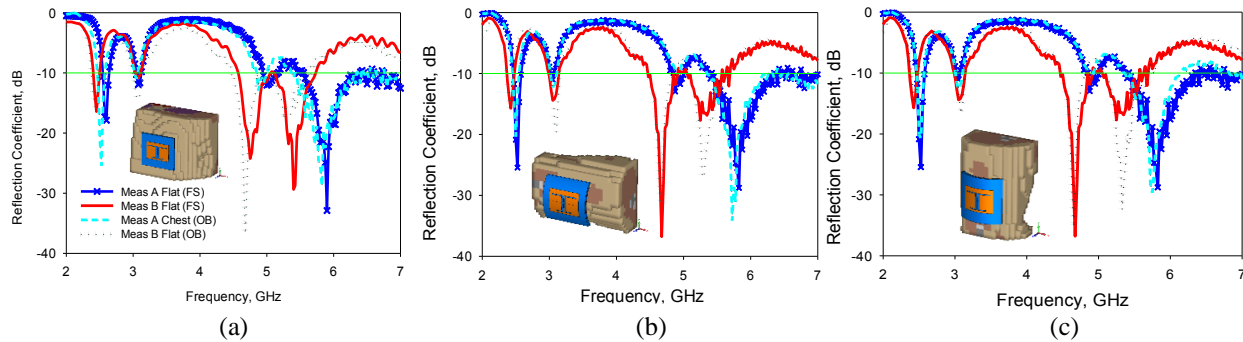


Fig. 7. Measured reflection coefficients of Antenna A and B when (a) placed on body (flat on chest and flat in free space), (b) bent with $X60$ on the upper arm, and (c) bent with $Y60$ on the upper arm. Legend: Crossed (blue) line: Antenna A flat on chest, solid (red) line: Antenna B flat on chest, short dashed (cyan) line: Antenna A in $X60$ and $Y60$ conditions and dotted (black) line: Antenna B in $X60$ and $Y60$ conditions.

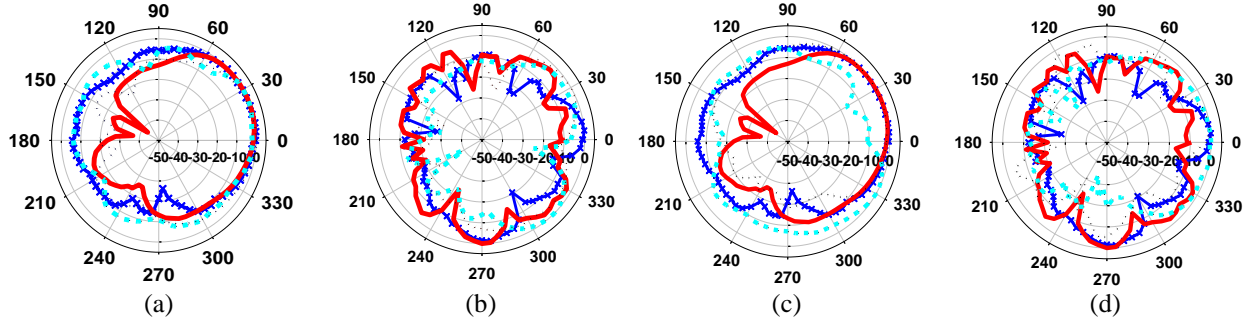


Fig. 8. Normalized measured radiation patterns for Antenna A and B when placed flat on chest and bent with $X60$ and $Y60$ on body: (a) at 2.45 GHz in the xz -plane ($X60$), (b) at 5.8 GHz in the xz -plane ($X60$), (c) at 2.45 GHz in the xz -plane ($X60$), (d) at 5.8 GHz in the xz -plane ($Y60$). Legend: Solid crossed (blue) line: Antenna A placed flat on chest, solid (red) line: Antenna B placed flat on chest, short dashed (cyan) line: Antenna A with $X60/Y60$ on the upper arm, and dotted (black) line: Antenna B with $X60/Y60$ on the upper arm.

Table 3: Summary of the tissue properties used in simulations

Tissue Type	Blood		Muscle		Fat	
	2.45	5.8	2.45	5.8	2.45	5.8
Frequency (GHz)	2.45	5.8	2.45	5.8	2.45	5.8
ϵ	58.3	52.5	52.7	48.49	5.28	4.95
$\tan\delta$	0.32	0.38	0.24	0.32	0.15	0.18
Cond (S/m)	2.54	6.51	1.74	4.96	0.10	0.29

Finally, the antennas bent at the x - and y -axes are experimentally validated in terms of reflection coefficient. This is performed similarly as was done in simulations using a thin and hollow cylinder on a human volunteer. The measured results illustrated in Figs. 7 (b) and (c) indicated that there is minimal level of changes in the lower band despite bending the antenna structure at both x - and y -axes. Changes are mainly noticeable in the upper band, where the same antenna (either A or B) maintaining their behavior despite being bent at different axes. This indicates that the antenna is affected minimally when bent at either axis.

D. Specific Absorption Rate (SAR)

The SAR values for both proposed antenna is calculated using CST MWS by placing the antennas in proximity of a truncated human voxel model (either on the chest or upper arm). Similar to the previous investigation [17], the antennas are placed 10 mm away from these models. The SAR value is calculated based on the IEEE C95.1 standard averaged over 10 g of tissue volume and is regulated to be safe when lower than 2 W/kg.

SAR is a measure of power absorbed per unit mass, e.g., in the human body tissue. It is spatially averaged

over the total mass of an exposed body or its parts, and it is calculated from the root-mean-square electric field strength, E (in volts per meter) inside the human body; the conductivity, σ (in Siemens per meter); and the mass density, ρ (in kilograms per cubic meter) of the biological tissue as follows:

$$SAR = \frac{\sigma E^2}{\rho}. \quad (1)$$

SAR is calculated by solving electromagnetic field interaction from different and adjacent meshes. In the case of the body tissues, their voxel properties were determined from MRI scans of different tissues. In this work, hexahedral meshes were used so that the constitutive parameters for each cell edge with irregular geometries and inhomogeneous dielectric composition can be calculated independently. Next, the simulator then solves the Maxwell's equations at each cell edge at discrete time steps, taking into consideration the three dimensional complex biological geometries, which involves a large amount of cells. In this work, SAR were calculated on the truncated chest and upper arm models with a total of about 20 million of hexahedral meshes per simulation. While meshes were generated automatically prior to simulations, at least 10 lines per wavelength with a mesh line ratio limit of 20 is set.

Table 4: Summary of the calculated SAR from both antennas

SAR Value	Chest (W/kg)		$X60$ on the Upper Arm (W/kg)		$Y60$ on the Upper Arm (W/kg)	
	2.45	5.8	2.45	5.8	2.45	5.8
Ant A	0.094	0.043	0.121	0.057	0.097	0.047
Ant B	0.082	0.052	0.122	0.061	0.089	0.059

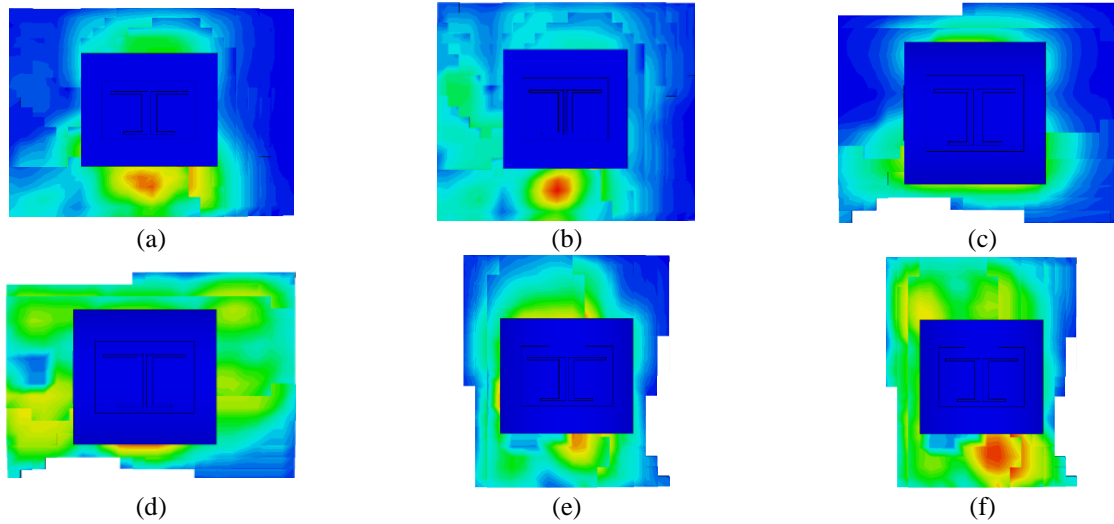


Fig. 9. Calculated SAR distribution for Antenna B when placed in planar and bent conditions at: (a) 2.45 GHz (flat), (b) 5.8 GHz (flat), (c) 2.45 GHz (with $X60$), (d) 5.8 GHz (with $X60$), (e) 2.45 GHz (with $Y60$), and (f) 5.8 GHz (with $Y60$).

Table 5: Comparison of the proposed antenna with recent literatures in terms of performance.

Ref. No.	Topology	Op. Bands (GHz)	10dB Frac. WBW (%)	Gain (dB)	10 dB BW Deviation on Body (GHz)	SAR (W/kg)
[2]	Planar dipole, fork shaped	2.4	12.7	4.9	0.3	1.98
		5.2	4.45	6.15	0.2	0.92
[3]	Planar slotted dipole	2.45	12.7	2.5	0.06	0.046
		5.2	18.9	0 to 4	0.2	0.023
[7]	Planar magneto-dielectric dipole	2.45	20	4.7	0.03	0.026
		5	31.5	3	0.05	0.044
[11]	Patch with metamaterial element	2.45	5.5	-3.5	0.02	0.012
		5.14	11.3	6.6	0.2	0.25
Ant B	Planar slotted dipole	2.45	4.11	5.9	0.05	0.082
		5.8	13.12	7.2	0.05	0.052

A summary of the SAR values calculated for both antennas is provided in Table 4. The calculated SAR distribution at 2.45 GHz and 5.8 GHz for Antenna B when placed in all three configurations (flat, $X60$ and $Y60$) are shown in Fig. 9. Due to the use of the AMC plane, the SAR values for both antennas did not exceed 0.13 W/kg in all bands. It can be seen that SAR values for both antennas are similar when placed on all locations and for all configurations. It is also observed that the highest SAR is produced in the lower band when bent in $X60$ condition for both antennas. The proposed antenna is compared with recent textile antennas operating in dual band mode and is summarized in Table 5. It can be observed that Antenna B provided comparable, if not better, balance in performance between bandwidth and gain, besides the reasonably low SAR when operated on body.

IV. CONCLUSIONS

A dual band slotted dipole antenna with AMC is proposed for operation in the 2.45 GHz and 5.8 GHz for WLAN and WBAN bands. To ensure a flexible, wearable and low profile structure, felt is used as its substrate and ShieldIt Super as its conductors. The proposed Antenna B is compared with a previous work denoted as Antenna A. It is observed that the integration of Antenna B with the optimized AMC produced wider bandwidths of 766 MHz (flat), 875 MHz ($X60$) and 850 MHz ($Y60$) in the upper band. In the lower band, both antennas produced similar narrow bandwidths of about 100 MHz. Despite this, Antenna B improved the realized gain and reduced backward radiation for all conditions relative to Antenna A. Maximum gains of 2.38 dB and 6.53 dB are observed in the lower and upper band, respectively, when assessed in a planar free space

condition. Higher directivities and gains are also observed for Antenna B in both bands. Finally, calculated SAR value using a detailed human body model for both antennas are below 0.13 W/kg indicating their safe operation in proximity of the human body in planar and bent conditions.

ACKNOWLEDGEMENTS

This work is supported in part by the Fundamental Research Grant Scheme (FRGS) (grant no 9003-00527), the MyBrain Scholarship, both from the Malaysian Ministry of Higher Education (MOHE); and the Thailand Research Fund through the TRF Senior Research Scholar Program under Grant RTA 6080008.

REFERENCES

- [1] P. J. Soh, F. N. Gimán, M. F. Jamlos, H. Lago, and A. A. Al-Hadi, "A C-slotted dual band textile antenna for WBAN applications," *IEEE URSI Asia-Pacific Radio Science Conference (URSI AP-RASC)*, Fajardo, Puerto Rico, pp. 1621-1624, June 2016.
- [2] A. Afridi, S. Ullah, S. Khan, A. Ahmed, A. H. Khalil, and M. A. Tarar, "Design of dual band wearable antenna using metamaterials," *Journal of Microwave Power and Electromagnetic Energy*, vol. 47, no. 2, pp. 126-37, 2013.
- [3] S. Yan, P. J. Soh, and G. A. E. Vandenbosch, "Low-profile dual-band textile antenna with artificial magnetic conductor plane," *IEEE Transactions on Antennas and Propagation*, vol. 62, no. 12, pp. 6487-90, 2014.
- [4] H. Lago, J. P. Soh, M. F. Jamlos, et al., "Textile antenna integrated with compact AMC and parasitic elements for WLAN/WBAN applications," *Applied Physics A*, vol. 122, pp. 1059, 2016.
- [5] Z. H. Jiang, D. E. Brocker, P. E. Sieber, and D. H. Werner, "A compact, low-profile metasurface-enabled antenna for wearable medical body-area network devices," *IEEE Transactions on Antennas and Propagation*, vol. 62, no. 8, pp. 4021-30, 2014.
- [6] Y. H. Di, X. Y. Liu, and M. M. Tentzeris, "A conformable dual-band antenna equipped with AMC for WBAN applications," *IEEE Asia-Pacific Conference on Antennas and Propagation (APCAP)*, Harbin, China, pp. 388-391, July 2014.
- [7] S. Yan, P. J. Soh, and G. A. E. Vandenbosch, "Wearable dual-band magneto-electric dipole antenna for WBAN/WLAN applications," *IEEE Transactions on Antennas and Propagation*, vol. 63, no. 9, pp. 4165-4169, 2015.
- [8] Z. H. Jiang and D. H. Werner, "A metasurface-enabled low-profile wearable antenna," *IEEE Antennas and Propagation Society International Symposium (APSURSI)*, Memphis, USA, pp. 273-274, July 2014.
- [9] S. Zhu and R. Langley, "Dual-band wearable textile antenna on an EBG substrate," *IEEE Transactions on Antennas and Propagation*, vol. 57, no. 4, pp. 926-35, 2009.
- [10] A. Alermayeen and S. Noghianian, "AMC integrated textile monopole antenna for wearable applications," *ACES Journal*, vol. 31, no. 6, pp. 612-618, 2016.
- [11] S. Yan, P. J. Soh, and G. A. E. Vandenbosch, "Compact all-textile dual-band antenna loaded with metamaterial-inspired structure," *IEEE Antennas and Wireless Propagation Letters*, vol. 14, pp. 1486-9, 2015.
- [12] H. R. Khaleel, H. M. Al-Rizzo, and D. G. Rucker, "An AMC based antenna for telemedicine applications," *ACES Journal*, vol. 27, no. 2, pp. 59-66, 2012.
- [13] R. C. Hadarig, M. E. De Cos, and F. Las-Heras, "Microstrip patch antenna bandwidth enhancement using AMC/EBG structures," *International Journal of Antennas and Propagation*, pp. 1-6, 2012.
- [14] M. N. Pavan and N. Chattoraj, "Design and analysis of a frequency reconfigurable antenna using metasurface for wireless applications," *IEEE International Conference on Innovations in Information, Embedded and Communication Systems (ICIECS)*, Coimbatore, India, pp. 1-5, Aug. 2015.
- [15] V. Kumar and B. Gupta, "On-body measurements of SS-UWB patch antenna for WBAN applications," *AEU-International Journal of Electronics and Communications*, vol. 70, no. 5, pp. 668-675, 2016.
- [16] S. Gabriel, R. W. Lau, and C. Gabriel, "The dielectric properties of biological tissues III: Parametric models for the dielectric spectrum of tissues," *Physics in Medicine and Biology*, vol. 41, no. 11, pp. 2271-93, 1996.
- [17] P. J. Soh, G. A. E. Vandenbosch, F. H. Wee, et al., "Specific absorption rate (SAR) of textile antennas," *IEEE Antennas and Propagation Magazine*, vol. 57, no. 2, pp. 229-240, 2015.